ISSN 0031-918X, Physics of Metals and Metallography, 2021, Vol. 122, No. 10, pp. 1014–1022. © Pleiades Publishing, Ltd., 2021.
Russian Text © The Author(s), 2021, published in Fizika Metallov i Metallovedenie, 2021, Vol. 122, No. 10, pp. 1091–1100.

## STRENGTH AND PLASTICITY

# Microstructure and Impact Toughness of High-Strength Low-Alloy Steel after Tempforming

**A. S. Dolzhenko[a], *, P. D. Dolzhenko[a], A. N. Belyakov[a], and R. O. Kaibyshev[a]**

[a] *Belgorod State University, Belgorod, 308015 Russia*

**e-mail: dolzhenko_a@bsu.edu.ru*

Received April 9, 2021; revised June 16, 2021; accepted June 18, 2021

**Abstract**—The effects of temperature and degree of tempforming deformation on the microstructure and impact toughness of high-strength low-alloy 25KhGMT steel have been considered. Tempforming forms a lamellar microstructure composed of grains and subgrains that are strongly elongated along the rolling direction. The average size of the grain section is 570–790 nm. Deformation texture includes ⟨001⟩ ∥ ND and ⟨111⟩ ∥ ND fibers. Tempforming increases the fracture work of this steel at lower test temperatures ($KV_{-40^\circ C} \geq 360$ J) due to the delamination of the specimen perpendicular to the impact direction, which prevents crack propagation towards the direction of the impact.

**Keywords:** tempforming, lamellar structure, impact toughness, fractography

**DOI:** 10.1134/S0031918X21100021

## INTRODUCTION

Low-alloy steels are widely used as structural materials in building and mechanical engineering. Massive commercial implementation of thermomechanical controlled processing (TMCP) has greatly reduced the cost of these steels, therefore considerably expanding their application fields [1]. Among their disadvantages is their relatively high brittle-ductile transition temperature (BDT) after quenching and tempering or TMCP, which makes these steels brittle and limits their application below zero degree Celsius. The nature of BDT is currently explained in terms of the Ioffe diagram, according to which an increase in the brittle fracture resistance and/or a decrease in the effective yield strength decreases the BDT temperature [2]. The latest studies have shown that the Ioffe scheme describes BDT in a simplified way [3–5]. The impact toughness can be increased and the BDT temperature can be lowered by increasing the critical crack length and, accordingly, the length of the stage of stable crack propagation via ductile fracture or mixed brittle-ductile fracture mechanism [3–7].

The traditional approach to suppress brittle intergranular fracture involves grain refinement and precipitation of dispersed particles along grain boundaries that retard the propagation of the intergranular crack [4, 8]. On the other hand, delamination of the material across the crack propagation direction blunts the crack tip and thus increases the fracture toughness [9]. The crack does not reach the critical size, and the stage of unstable crack propagation does not occur. The hypereutectoid low-alloy steel plates fabricated by isothermal rolling of a multilayer pack at 650°C, and the composite consisting of alternating layers of this steel and low-carbon 08 grade steel demonstrated an ultrahigh impact toughness $KCV > 250$ J/cm$^2$ at −125°C [10].

Kimura and coauthors used the effect of transverse crack delamination in V-notch specimens that was called “delamination toughness,” to increase the impact toughness and decrease the brittle-ductile transition temperature of 40KhS2M steel [11]. The proposed approach is to use warm rolling to form a submicrocrystalline fiber structure with uniformly distributed carbide particles at the temperature of the tempering of martensite-hardened steel. This treatment, called tempforming [12], provides a unique combination of high strength and toughness in low-alloyed medium-carbon steels. The efficiency of tempforming, when compared to tempering after quenching at the same temperature that can be estimated by the ratio of impact toughness *KCV* to ultimate strength, increases with decreasing carbon content for different steels [13]. In addition, a decrease in the tempforming temperature makes the effect of delamination toughness more pronounced in low-alloy low-carbon steels, whereas the tempforming temperature in medium-carbon steels has no significant effect on the impact toughness. The lack of systematic experimental studies is the reason why the reg-

**Table 1.** Microstructural parameters of the 25KhGMT steel after different tempforming regimes

| State | Subgrain size, μm | Grain size, μm | Fraction of HABs | $\rho \times 10^{14}$, $m^{-2}$ |
|---|---|---|---|---|
| $T_{TF} = 600°C$, $e = 0.8$ | 0.9 ± 0.1 | 1.4 ± 0.1 | 0.46 ± 0.05 | 7.1 ± 0.1 |
| $T_{TF} = 650°C$, $e = 0.8$ | 1.1 ± 0.1 | 1.6 ± 0.1 | 0.55 ± 0.05 | 7.4 ± 0.1 |
| $T_{TF} = 600°C$, $e = 1.4$ | 0.45 ± 0.05 | 0.57 ± 0.05 | 0.71 ± 0.05 | 6 ± 0.1 |
| $T_{TF} = 650°C$, $e = 1.4$ | 0.55 ± 0.05 | 0.79 ± 0.05 | 0.59 ± 0.05 | 8 ± 0.1 |

ularities of tempforming-induced changes in the steel properties cannot be established. This work aims to study the deformation degree of the tempforming performed at various temperatures on the microstructure and mechanical properties of the 25KhGMT steel.

## EXPERIMENTAL

The object of the investigation was high-strength low-alloy 25KhGMT steel with the following chemical composition (wt %): 0.26 C, 0.23 Si, 0.54 Mn, 0.42 Cr, 0.44 Mo, 0.06 Ti, and Fe for balance. The steel was preliminarily subjected to quenching at 850°C and water cooling. Tempforming included heating the steel billets in a muffle furnace to the tempering temperature (600, 650°C), keeping them at this temperature for 1 h, and then rolling them in several passes to a true strain of 0.8 and 1.4. The reduction per pass was 10%. After each pass, a steel billet was heated to the tempering temperature.

The microstructural examination was carried out using Quanta Nova Nanosem 450 FEG scanning electron microscope (SEM) equipped with a back-scattering electron diffraction (EBSD) detector, and using TSL OIM Analysis 6 software. The orientation imaging microscopy (OIM) images were cleaned by removing points with a confidence index of less than 0.1. The average cross-sectional size of grains and subgrains was estimated using OIM (orientation distribution map) images as the average distance between the high-angle boundaries (HABs) with misorientations $\theta \geq 15°$ and the low-angle boundaries (LABs) with misorientations $\theta \geq 2°$, respectively, in the direction normal to the rolling plane. The fine structure was examined using a JEOL JEM-200 transmission electron microscope at an accelerating voltage of 200 kV. Foils for microstructure examination were prepared by jet polishing technique in a 10% solution of perchloric acid in acetic acid using a Struers Tenupol 5 equipment.

Standard square-section specimens $10 \times 10$ $mm^2$ in size and 55 mm in length with a V-notch stress concentrator were tested for the impact toughness in the temperature range from 20 to −196°C using an Instron 450 J machine equipped with an Instron Dynatup Impulse data acquisition system. One specimen per point was tested. Specimens for impact toughness tests were cut so that the impact direction was parallel to the normal rolling direction.

Fractographic studies after mechanical tests were performed using an FEI Quanta 200 scanning electron microscope.

## RESULTS AND DISCUSSION

**Steel microstructure after tempforming.** Figure 1 shows the microstructure of the 25KhGMT steel formed during tempforming at different temperatures and different deformation degrees.

Tempforming at temperatures ($T_{TF}$) 600 and 650°C to a true strain $e \sim 0.8$ results in the formation of grains elongated along the rolling direction (RD). The average cross-sectional grain sizes are 1.4 and 1.6 μm, respectively. The dislocation density was calculated by the formula (1) [14]. The results of the calculation and microstructural parameters are shown in Table 1.

$$\rho = \frac{2\theta_{KAM}}{bh}, \quad (1)$$

where $\theta_{KAM}$ is the average lattice curvature around each scanning point for the first coordination sphere, $b$ is the Burgers vector, and $h$ is the step of scanning.

A submicrocrystalline lamellar structure, consisting of strongly elongated grains along the rolling direction, forms at the strain $e \sim 1.4$. The cross-sectional grain size decreases to 570 nm at $T_{TF} = 600°C$ and 790 nm at $T_{TF} = 650°C$ (Table 1). The test specimens exhibit a high dislocation density of more than $5 \times 10^{14}$ $m^{-2}$ that weakly depends on temperature and deformation degree. This behavior is typical of warm deformation performed to large degrees that may be accompanied by some decrease in the density of intragrain dislocations with increasing deformation degrees [15]. The 25KhGMT steel after tempforming to $e \sim 1.4$ has a fiber deformation texture of $\langle 001 \rangle \parallel$ ND and

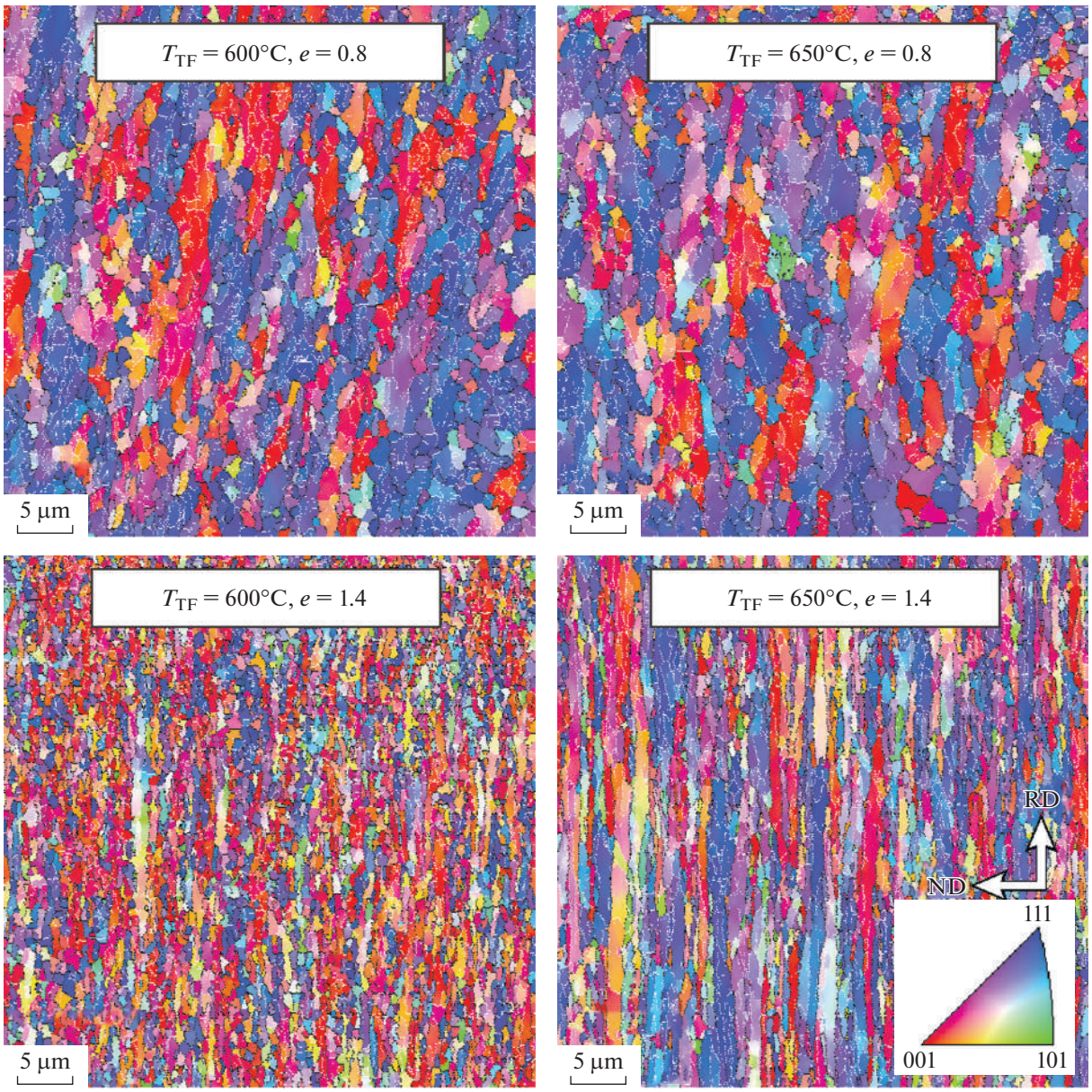


**Fig. 1.** Microstructure of the 25KhGMT steel after various tempforming regimes (EBSD maps of crystallographic orientations).

⟨111⟩ ∥ ND, in favor of which the predominance of red and blue colors in the map of crystallographic orientations counts (Fig. 1).

Figure 2 shows the fine structure after tempforming to $e \sim 1.4$ at temperatures of 600 and 650°C that is characterized by a layered substructure with an average subgrain cross-sectional size of 450 and 550 nm, respectively (Table 1).

The tempforming of the 25KhGMT steel is accompanied by the formation of carbides (cementite and $Cr_{23}C_6$, about 2% each, according to Thermo-Calc, TCFE7) mainly at grain boundaries/subgrain boundaries in the ferritic matrix. Their sizes range from 10 to 100 nm. Carbides after tempforming are uniformly distributed. However, particles formed at HABs are relatively coarse, whereas those formed at LABs are smaller significantly.

**Impact toughness and fractography.** Figure 3 shows the tempformed 25KhGMT steel specimens after impact toughness tests in a wide temperature range. The work of fracture (*KV*) is indicated in the figure.

Almost all specimens under study after tempforming to $e \sim 0.8$ show complete failure after the impact strength test over the entire temperature range (except for specimens at $T_{TF}$ = 600°C, $e \sim 0.8$, and $T_{TF}$ = 650°C, $e \sim 0.8$ in the –90°C test). The hinged and par-

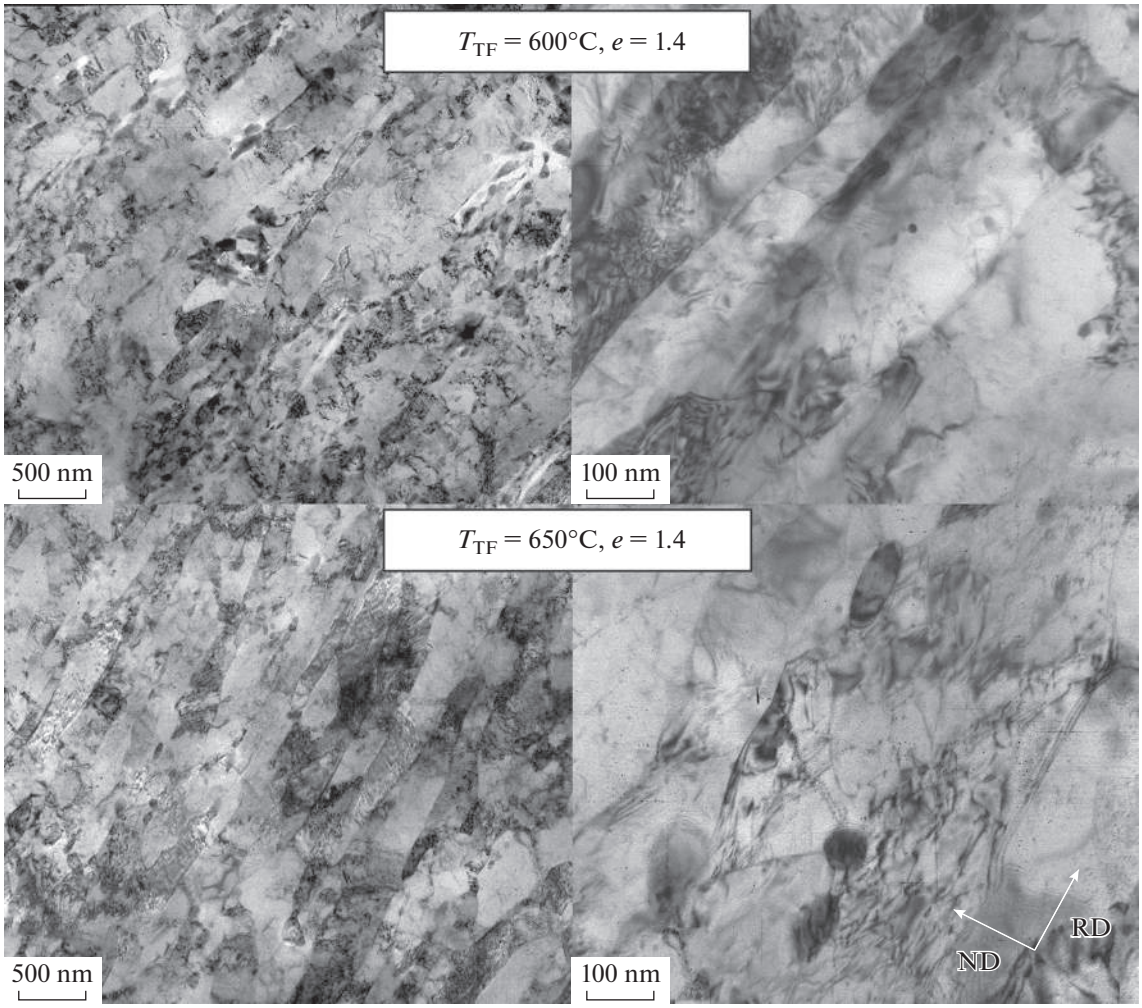


**Fig. 2.** Fine structure of the 25KhGMT steel after different tempforming regimes.

tial fracture is observed in the specimens after tempforming to $e \sim 1.4$, which indicates higher absorbed impact energy [7]. We should note that the 25KhGMT steel specimens tempformed to $e \sim 1.4$ do not lose their ability to delamination and keep their fracture work *KV* above 200 J even at the temperature of liquid nitrogen boiling (–196°C), in contrast to the specimens tempformed to $e \sim 0.8$ when the specimens are destroyed by a zigzag cracking and their fracture work does not exceed 10 J.

The steel specimens after tempforming to $e \sim 0.8$ (Fig. 4) exhibit ductile fracture at room temperature and a typical pattern of flat pits [7, 16]. The fracture mechanism changes to brittle with decreasing test temperature, which is indicated by the presence of cleavage facets. The fracture pattern of the specimens after impact toughness tests at temperatures below –40°C becomes mixed, namely, both pits and facets are observed. The fracture pattern becomes completely brittle at a test temperature of –196°C.

Figures 5 and 6 show the fracture surfaces of the steel tempformed to $e \sim 1.4$ after the impact strength tests at temperatures of 20, –40, and –196°C. The figures include fracture surfaces resulted from crack propagation along the impact direction, i.e., perpendicular to the specimen (Figs. 5a, 5c, 5e, 6a, 6c, 6e), and from crack propagation perpendicular to the impact direction, i.e., along the specimen (Figs. 5b, 5d, 5f, 6b, 6d, 6f). Irrespective of the temperature of tempforming (to $e \sim 1.4$), the 25KhGMT steel fractures in the same mechanisms and exhibits the same fracture surfaces over the entire temperature range of the tests. The fracture mechanisms in all specimens depend significantly on the direction of crack propagation. The fracture surfaces that result from crack propagation towards the impact direction show typical ductile fracture with dimpled failure.

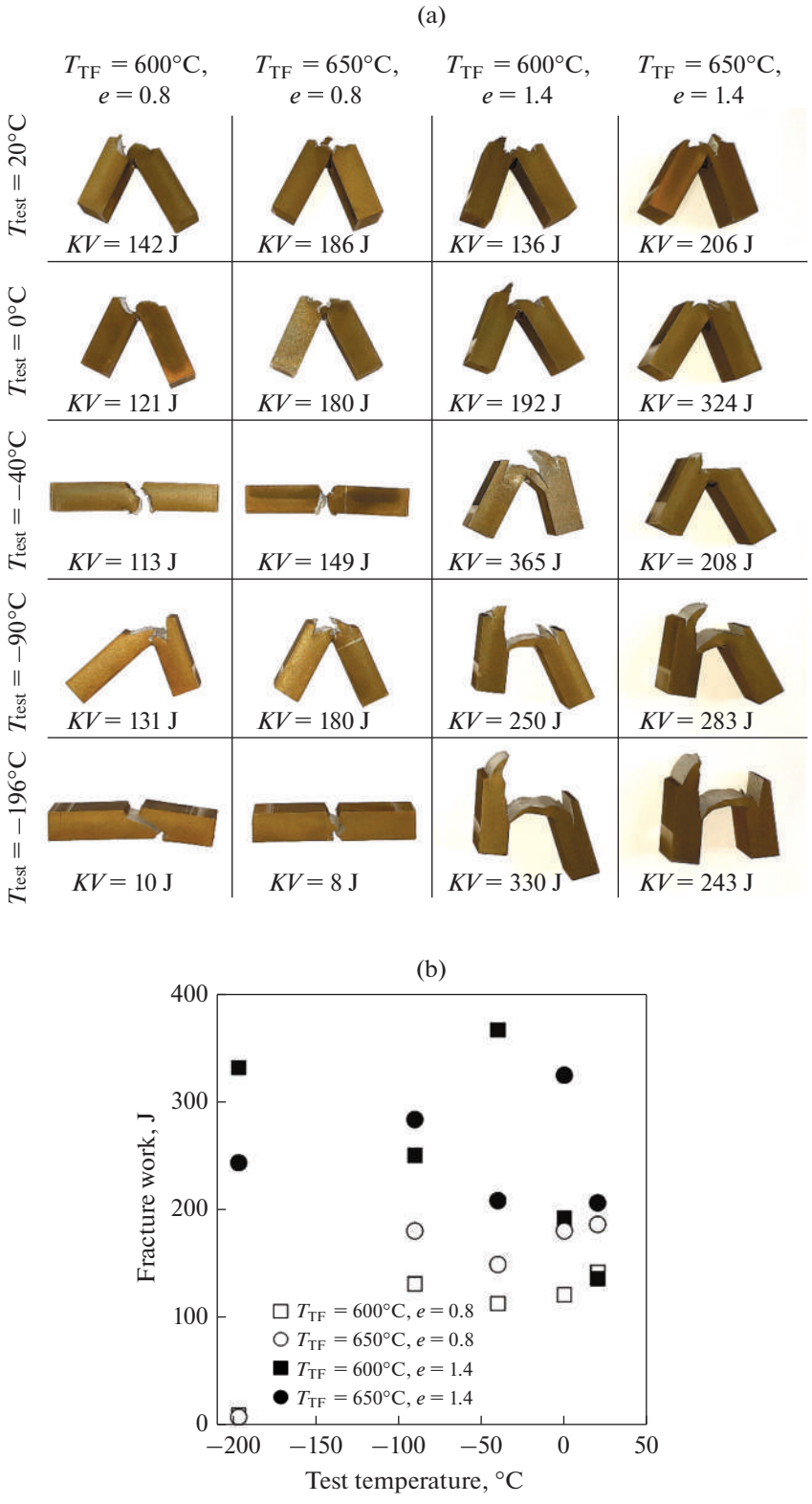


**Fig. 3.** (a) Impact toughness and (b) fracture work as a function of temperature for the 25KhGMT steel specimens after temp-forming.

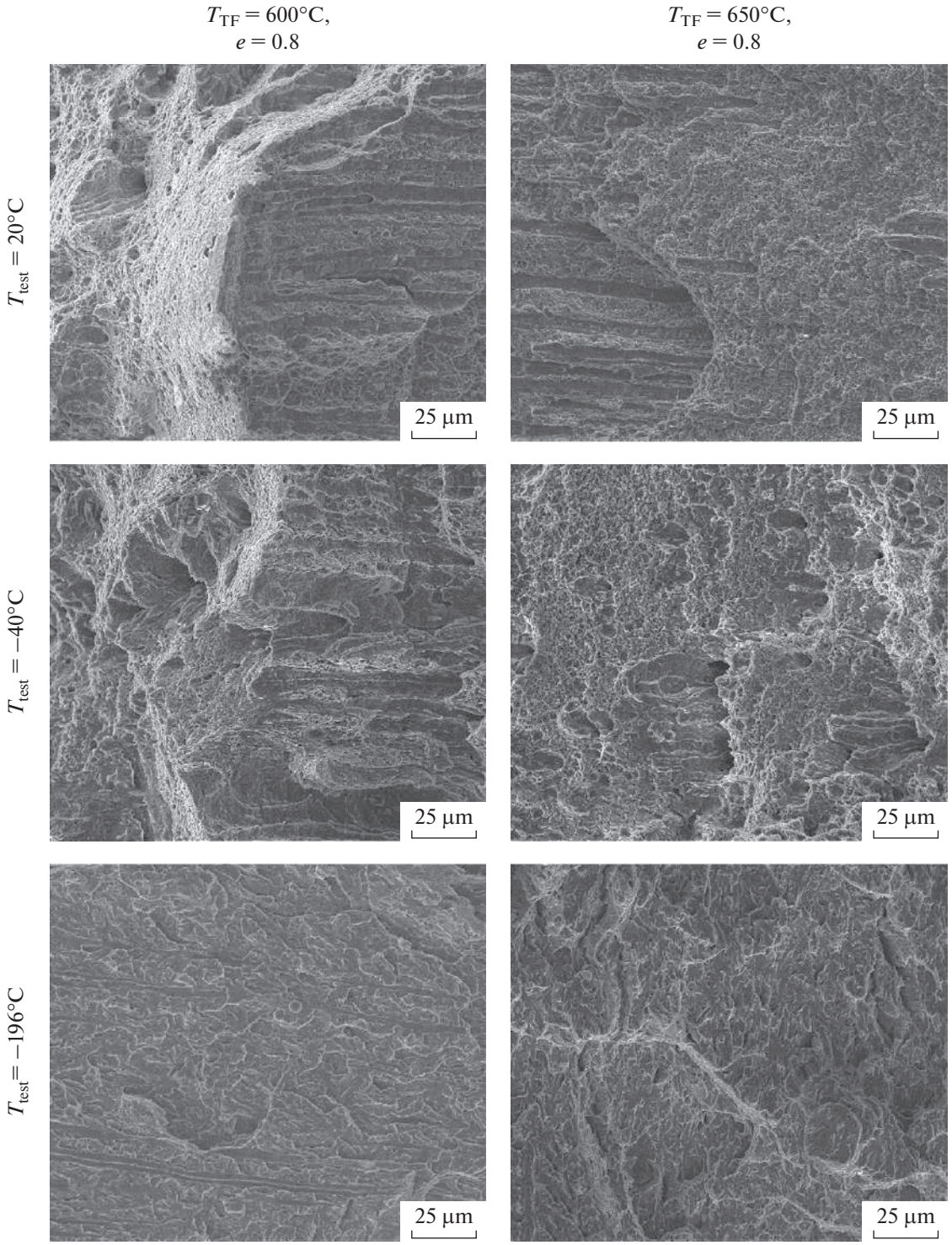


**Fig. 4.** Fracture patterns of the 25KhGMT steel that was subjected to tempforming at different temperatures to the true strain of 0.8, after impact toughness tests at various temperatures.

On the other hand, fracture surfaces caused by cracking perpendicular to the impact direction are characterized by brittle fracture, which is indicated by cleavage facets.

Transcrystalline fracture in all specimens in Figs. 5 and 6 is characterized by crack propagation over a large distance, which results in a huge fracture surface area. This is typical of the ductile delamination phe-

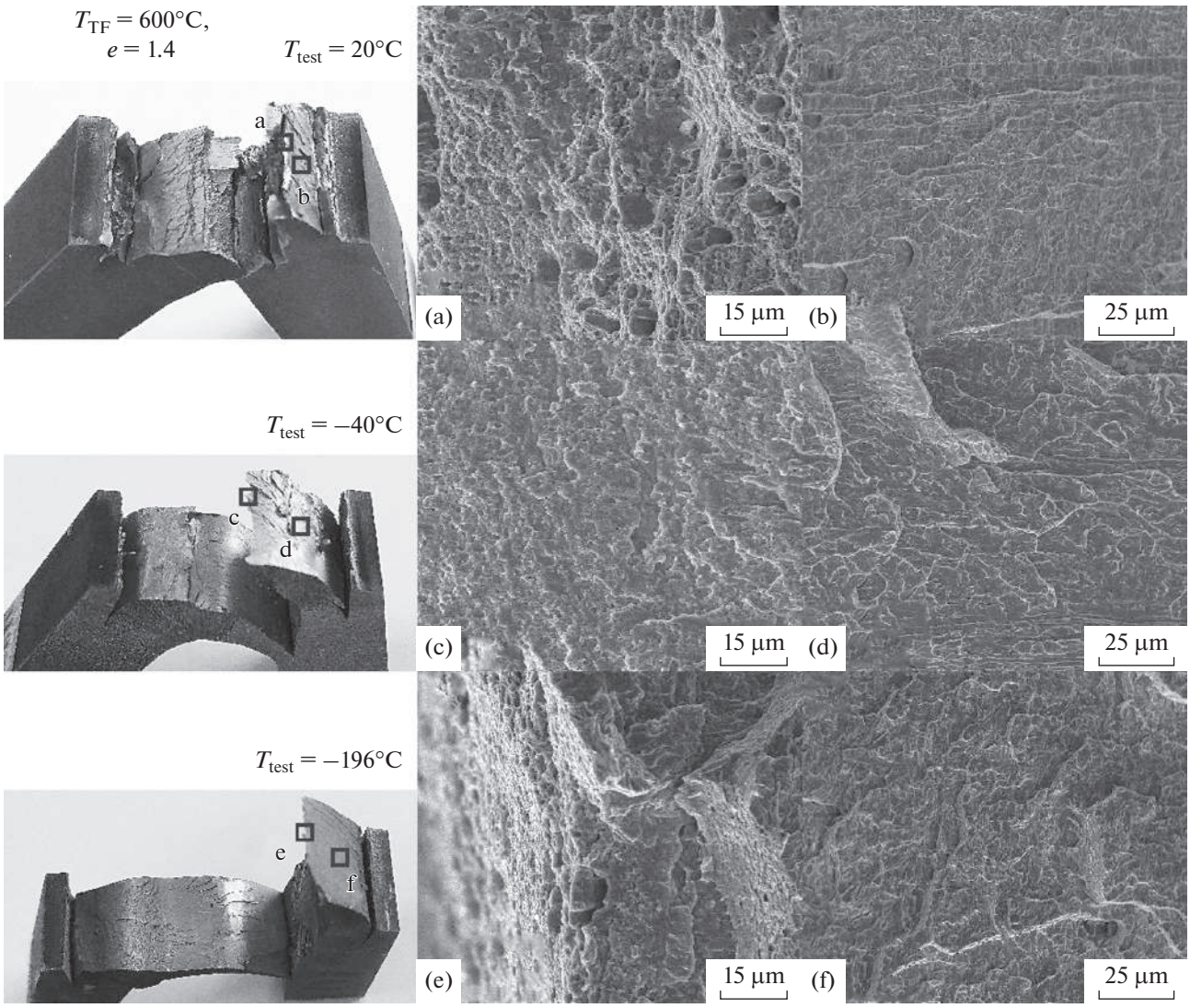


**Fig. 5.** Fracture patterns of the 25KhGMT steel that was subjected to tempforming at 600°C to the true strain of 1.4, after impact toughness tests at various temperatures. (a), (c), (e) crack propagation towards impact direction, and (b), (d), (f) crack propagation perpendicular to the impact direction.

nomenon, where a cleavage that is perpendicular to the impact direction prevents crack propagation along the impact direction and, therefore, increases impact toughness due to an increase in absorbed energy.

The unusual increase in the impact toughness with decreasing test temperature after tempforming to $e \sim 1.4$ is explained by the difference in the coherent cleavage plane lengths along and across the specimen ($L_{ND}$, $L_{RD}$ in Fig. 7) [17, 18]. The coherence length of the {001} cleavage planes in the tempformed steels is maximum in the rolling direction ($L_{ND}$) and minimum in the transverse direction ($L_{RD}$). Correspondingly, the cleavage fracture stress in the transverse direction ($\sigma_{C//ND}$ in Fig. 7) is minimal, while that along the rolling direction ($\sigma_{C//RD}$) is maximum. This difference increases with increasing deformation degree during tempforming. The yield strength ($\sigma_y$) is characterized by a similar anisotropy, but its variation is significantly smaller. However, $\sigma_y$ is strongly dependent on the temperature. The change in the fracture mechanism that was caused by the temperature decrease, and the transition from range I to range II (Fig. 7) are accompanied by an increase in the impact toughness, which occurs due to delamination along the specimen when $\sigma_y$ exceeds $\sigma_{C//ND}$. When the temperature decreases further, the impact toughness drops when $\sigma_y$ becomes greater than $\sigma_{C//RD}$.

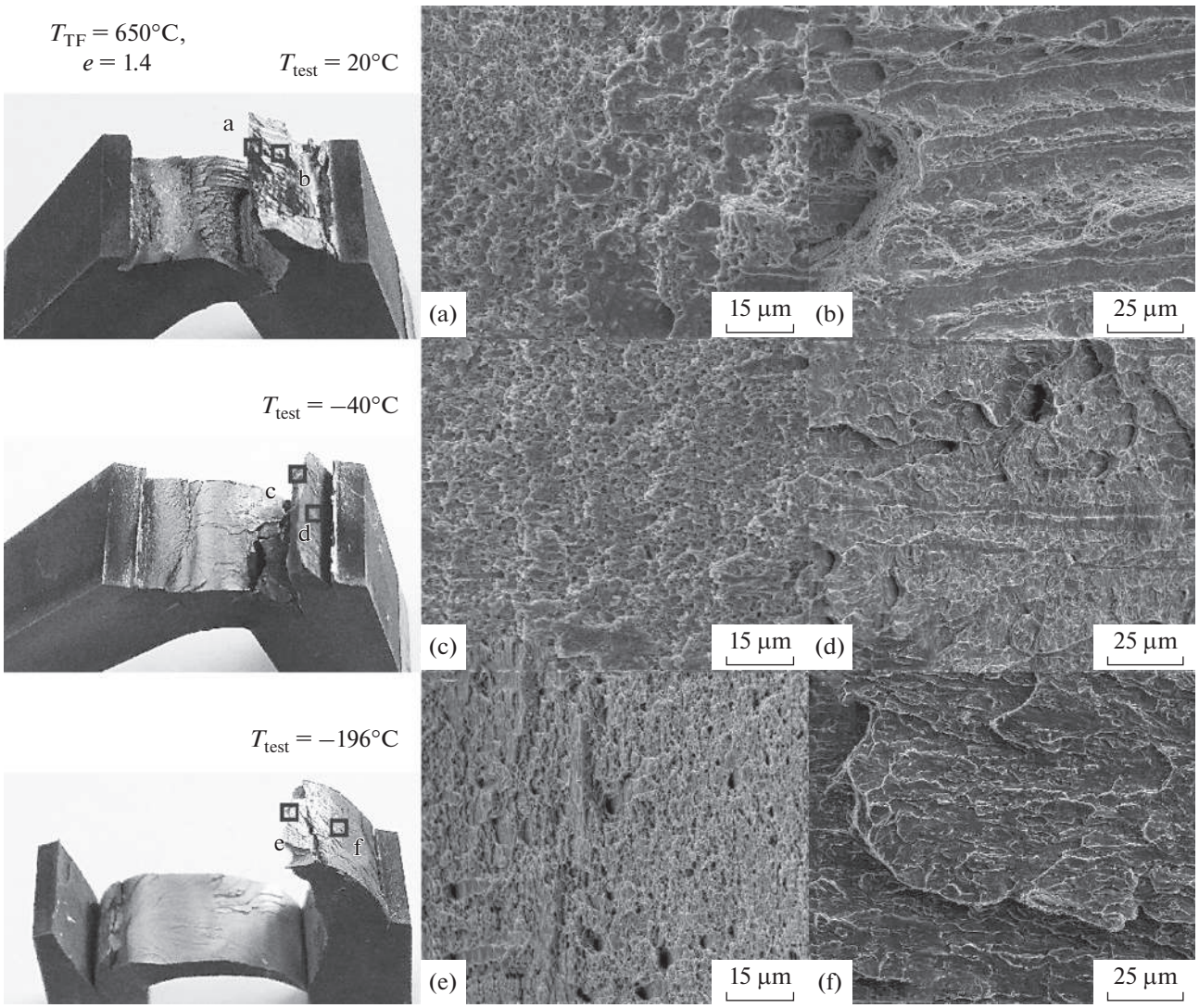


**Fig. 6.** Fracture patterns of the 25KhGMT steel that was subjected to tempforming at 650°C to the true strain of 1.4, after impact toughness tests at various temperatures. (a), (c), (e) crack propagation towards impact direction, and (b), (d), (f) crack propagation perpendicular to the impact direction.

## CONCLUSIONS

(1) The tempforming of the 25KhGMT steel at temperatures of 600 and 650°C results in the formation of the lamellar microstructure with elongated grains along the rolling direction. The cross-sectional grain size decreases from 1.4 to 0.57 μm at 600°C and from 1.6 to 0.79 μm at 650°C during tempforming when the strain increases from 0.8 to 1.4. The test specimens after tempforming to $e \sim 1.4$ exhibit a fiber deformation texture of $\langle 001 \rangle \parallel$ ND and $\langle 111 \rangle \parallel$ ND. The tempforming is accompanied by the precipitation of carbides 10 to 100 nm in size mainly at grain boundaries/subgrain boundaries.

(2) Tempforming of the 25KhGMT steel specimens to $e \sim 0.8$ keeps the fracture work at the level characteristic of the room test temperature when the test temperature drops to –90°C, while the fracture work increases with increasing the tempforming temperature. Increasing the strain to 1.4 increases the fracture work that tends to increase as the test temperature decreases. This unusual increase in the fracture work is caused by the delamination of the steel specimens along the direction perpendicular to the impact direction. At –196°C, specimens tempformed to $e \sim 1.4$ have *KV* values higher than 200 J, in contrast to the specimens tempformed to $e \sim 0.8$ that fracture through zigzag cracking, and their *KV* value does not exceed 10 J.

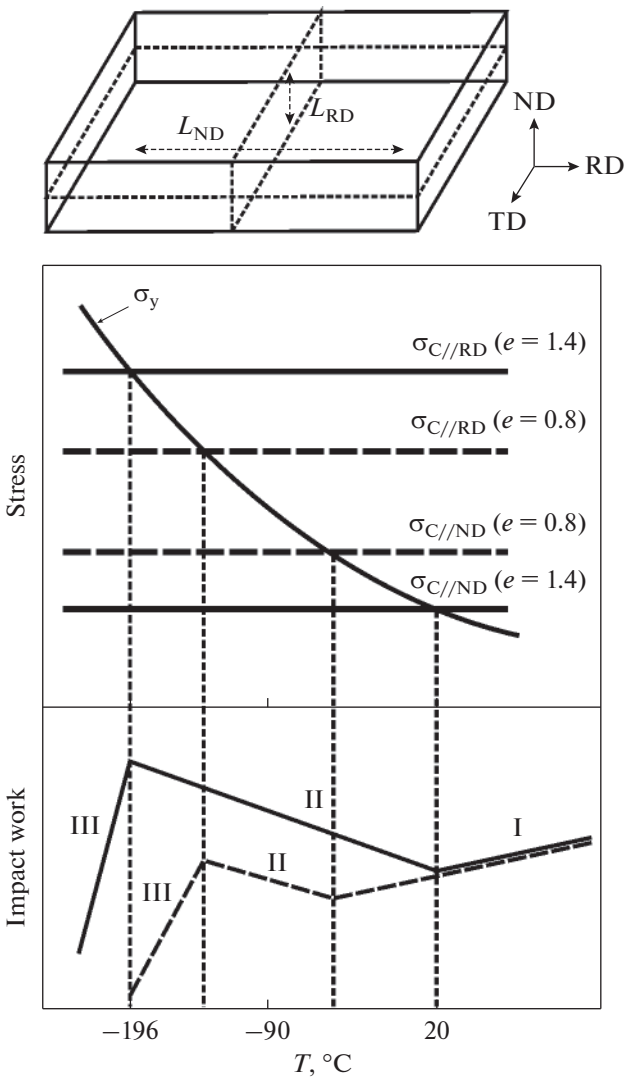


**Fig. 7.** Modified Ioffe diagram for steels with a lamellar structure after tempforming: (I) ductile fracture region, (II) delamination, and (III) brittle fracture.

## FUNDING

This work was supported by the Russian Scientific Foundation, project no. 20-19-00497. The structural examination and mechanical tests were performed at the Center of the Collaborative Access "Technologies and Materials," Belgorod State University.

## REFERENCES

1. K. Nishioka and K. Ichikawa, "Progress in thermomechanical control of steel plates and their commercialization," Sci. Technol. Adv. Mater. **13**, No. 2, 023001 (2012).
2. J. W. Morris, "Stronger, tougher steels," Science **320**, No. 5879, 1022–1023 (2008).
3. R. Mishnev, N. Dudova, V. Dudko, and R. Kaibyshev, "Impact toughness of a 10% Cr steel with high boron and low nitrogen contents," Mater. Sci. Eng., A **730**, 1–9 (2018).
4. J. Borisova, V. Dudko, R. Mishnev, and R. Kaibyshev, "Effect of laves phase on ductile-brittle transition of 12 Pct Cr steel," Metall. Mater. Trans. A **50**, 3528–3543 (2019).
5. R. Mishnev, N. Dudova, R. Kaibyshev, and A. Belyakov, "On the fracture behavior of a creep resistant 10% Cr steel with high boron and low nitrogen contents at low temperatures," Materials **13**, No. 1, 3 (2020).
6. R. Chaouadi and A. Fabry, "On the utilization of the instrumented Charpy impact test for characterizing the flow and fracture behavior of reactor pressure vessel steels," ESIS Publ. **30**, 103–117 (2002).
7. *ASM Handbook: Mechanical Testing and Evaluation* (ASM International Materials Park, 2000), Vol. 8, p. 2235.
8. A. Dolzhenko, R. Kaibyshev, and A. Belyakov, "Tempforming as an advanced processing method for carbon steels," Metals **10**, No. 12, 1566 (2020).
9. C. M. Yen and C. A. Stickels, "Lamellate fracture in 5150 steel processed by modified ausforming," Metall. Trans. **1**, No. 11, 3037–3047 (1970).
10. D. W. Kum, T. Oyama, J. Wadsworth, and O. D. Sherby, "The impact properties of laminated composites containing ultrahigh carbon (UHC) steels," J. Mech. Phys. Solids **31**, No. 2, 173–186 (1983).
11. Y. Kimura, T. Inoue, F. Yin, and K. Tsuzaki, "Inverse temperature dependence of toughness in an ultrafine grain-structure steel," Science **320**, No. 5879, 1057–1060 (2008).
12. Y. Kimura, T. Inoue, F. Yin, O. Sitdikov, and K. Tsuzaki, "Toughening of a 1500 MPa class steel through formation of an ultrafine fibrous grain structure," Scr. Mater. **57**, No. 6, 465–468 (2007).
13. Y. Kimura and T. Inoue, "Influence of carbon content on toughening in ultrafine elongated grain structure steels," ISIJ Int. **55**, No. 5, 1135–1144 (2015).
14. M. Calcagnotto, D. Ponge, E. Demir, and D. Raabe, "Orientation gradients and geometrically necessary dislocations in ultrafine grained dual-phase steels studied by 2D and 3D EBSD," Mater. Sci. Eng., A **527**, 2738–2746 (2010).
15. A. N. Belyakov, "Changes in the grain structure of metallic materials upon plastic treatment," Phys. Met. Metallogr. **108**, No. 4, 390–400 (2009).
16. A. Fedoseeva, N. Dudova, and R. Kaibyshev, "Role of tungsten in the tempered martensite embrittlement of a modified 9 pct Cr steel," Metall. Mater. Trans. A **48**, No. 3, 982–998 (2017).
17. Y. Kimura and T. Inoue, "Influence of warm tempforming on microstructure and mechanical properties in an ultrahigh-strength medium-carbon low-alloy steel," Metall. Mater. Trans. A **44**, No. 1, 560–576 (2013).
18. X. Min, Y. Kimura, T. Kimura, and K. Tsuzaki, "Delamination toughening assisted by phosphorus in medium-carbon low-alloy steels with ultrafine elongated grain structures," Mater. Sci. Eng., A **649**, 135–145 (2016).

*Translated by T. Gapontseva*